





Article

# Silver Nanoparticle-Intercalated Cotton Fiber for Catalytic Degradation of Aqueous Organic Dyes for Water Pollution Mitigation

Matthew Blake Hillyer , Jacobs H. Jordan , Sunghyun Nam \*, Michael W. Easson  and Brian D. Condon

Cotton Chemistry and Utilization Research Unit, Southern Regional Research Center, Agricultural Research Service, United States Department of Agriculture, New Orleans, LA 70113, USA; matthew.hillyer@usda.gov (M.B.H.); jacobs.jordan@usda.gov (J.H.J.); michael.easson@usda.gov (M.W.E.); brian.condon@usda.gov (B.D.C.)

\* Correspondence: sunghyun.nam@usda.gov; Tel.: +1-(504)-286-4229

**Abstract:** Azo dyes are commonly used in textile color processing for their wide array of vibrant colors. However, in recent years these dyes have become of concern in wastewater management given their toxicity to humans and the environment. In the present work, researchers remediated water contaminated with azo dyes using silver nanoparticles (Ag NPs) intercalated within cotton fabric as a catalyst, for their enhanced durability and reusability, in a reductive degradation method. Three azo dyes—methyl orange (MO), Congo red (CR), and Chicago Sky Blue 6B (CSBB)—were investigated. The azo degradation was monitored by UV/vis spectroscopy, degradation capacity, and turnover frequency (TOF). The Ag NP–cotton catalyst exhibited excellent degradation capacity for the dyes, i.e., MO (96.4% in 30 min), CR (96.5% in 18.5 min), and CSBB (99.8% in 21 min), with TOFs of 0.046 min<sup>-1</sup>, 0.082 min<sup>-1</sup>, and 0.056 min<sup>-1</sup>, respectively, using a 400 mg loading of catalyst for 100 mL of 25 mg L<sup>-1</sup> dye. To keep their high reusability while maintaining high catalytic efficiency of >95% degradation after 10 cycles, Ag NPs immobilized within cotton fabric have promising potential as eco-friendly bio-embedded catalysts.

**Keywords:** catalysis; silver nanoparticles; environmental; health issues; pollution remediation; cotton fibers; water



**Citation:** Hillyer, M.B.; Jordan, J.H.; Nam, S.; Easson, M.W.; Condon, B.D. Silver Nanoparticle-Intercalated Cotton Fiber for Catalytic Degradation of Aqueous Organic Dyes for Water Pollution Mitigation. *Nanomaterials* **2022**, *12*, 1621. <https://doi.org/10.3390/nano12101621>

Academic Editors: Vicente Montes, Rafael Estevez, Manuel Checa and Alexey Pestryakov

Received: 29 March 2022

Accepted: 4 May 2022

Published: 10 May 2022

**Publisher's Note:** MDPI stays neutral with regard to jurisdictional claims in published maps and institutional affiliations.



**Copyright:** © 2022 by the authors. Licensee MDPI, Basel, Switzerland. This article is an open access article distributed under the terms and conditions of the Creative Commons Attribution (CC BY) license (<https://creativecommons.org/licenses/by/4.0/>).

## 1. Introduction

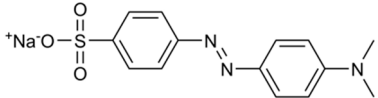
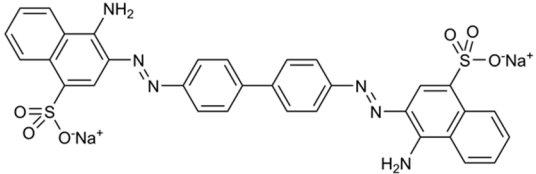
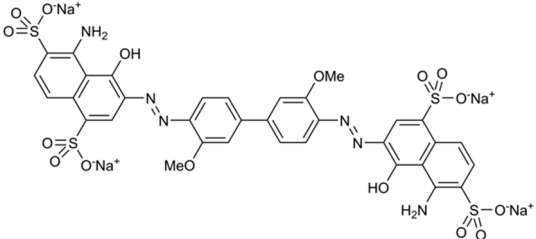
Increasing consumer demand for affordable apparel has put significant economic stress on textile processing, resulting in the dramatic rise of pollutants in wastewater effluent [1–3]. One of the major contaminants found in clothing manufacturing water discharge is organic dyes. All organic dye chemical structures are based on at least 1, up to a combination of 25, types of functional groups resulting in tens of thousands of possible chemical structures [4]. Of these many structures, the most common type used by material consumed in processing is azo-containing dyes. Azo dyes consist of at least one diazenyl (–N=N–) functional group. Total azo-dye use constitutes up to 70%, or 9 million tons, of total annual dye consumption worldwide [5,6]. Of this, 4.5 million tons of dye and dye degraded byproducts are disposed of annually, posing severe environmental and anthropogenic hazards.

There have been numerous studies showing the ecotoxicity of dyes in aquatic and terrestrial environments [7–12]. Water containing high concentrations of azo-dye decrease sun permeability, resulting in diminished photosynthesis by marine plants, significantly reducing the amount of available oxygen and causing ecosystem collapse [13]. Research focusing on specific micro- and macro-organisms found acute toxicity leading to chronic effects, including those caused by bioaccumulation, mutagenicity, and carcinogenicity [14–16]. Azo dyes can also be deleterious to human health via two modalities of exposure: skin contact

and ingestion [17]. Skin contact by azo dyes, specifically through colored garments, can cause allergic reactions, dermatitis, and skin irritation [18]. Ingestion of azo dyes causes damage to the endocrine and gastrointestinal systems and has been directly linked to several cancers, including those originating in the kidneys, liver, and bladder [17,19,20]. Therefore, there is great demand for an efficient and effective method to degrade azo dyes in industrial waste streams and municipal water sources.

Conventional industrial processes for the treatment of azo dye-contaminated wastewater include isolation (flocculation, coagulation, or membrane) or degradation (chemical or microbial) [21]. Isolation is often operationally costly and requires non-reusable coagulants or flocculants to form a physicochemical sludge [22]. This byproduct normally involves additional processing, further adding to the cost-prohibiting aspect. Recently, attention has been paid to using genetically engineered microorganisms as an avenue to remediate dye in industrial wastewater [23]. While this method generates a quantity of sludge, conditions must be kept optimal for microbe viability. Additionally, the process is often slow and the selectivity of certain molecules is often low. Alternatively, chemical degradation can be highly efficient and, with the application of catalysts, the reactions can proceed under mild conditions at ambient temperatures. There have been several studies investigating the highly effective degradation of azo dyes using silver nanoparticles (Ag NPs) [24–27]. While these methods are effective, they rely on using Ag NPs in free solution. Furthermore, the isolation and extraction of the catalyst presents a problem for cost-effective reusability. Herein, we present studies using a durable cotton-embedded Ag NP catalyst for the degradation of three azo dyes: methyl orange (MO), Congo red (CR), and Chicago Sky Blue 6B (CSBB) (Table 1). The capacity of the catalyst to be used over several iterations of the reaction cycle was investigated using simple extraction and isolation.

**Table 1.** Chemical and structural properties of azo dyes.

Dye	Molecular Weight (g/mol)	UV/Vis $\lambda_{\max}$ (nm)	Structure
Methyl Orange (MO)	327.33	464	
Congo Red (CR)	696.67	496	
Chicago Sky Blue 6B (CSBB)	992.80	618	

## 2. Materials and Methods

### 2.1. Chemicals

Silver nitrate (99.9999%, trace metal basis), ammonium hydroxide (40% *w/v*), sodium hydroxide (50% *w/v*), sodium borohydride ( $\geq 98\%$ ), Congo red (dye content  $\geq 85\%$ ), methyl orange (dye content 85%), Chicago Sky Blue B (dye content  $\sim 80\%$ ), methyl methacrylate, butyl methacrylate, and methyl ethyl ketone were purchased from Sigma-Aldrich (St. Louis, MO, USA). All chemicals were used without further purification. Bleached and desized

print cloth was purchased from Testfabrics, Inc. (West Pittston, PA, USA). Deionized water was used in the synthesis of Ag NPs in cotton textiles and in the preparation of dye solutions. All glassware was cleaned with 28% nitric acid and rinsed several times with deionized water.

## 2.2. Preparation and Characterization of Ag NP–Cotton Catalyst

The synthetic procedure for producing Ag NP-intercalated cotton fabric was used from a previously reported method [28]. A 5 cm × 10 cm specimen was immersed into 20 mL of an aqueous NaOH solution (20 *w/v*) and agitated at room temperature for 15 min. The excess NaOH solution was removed using a laboratory padder (Werner Mathis USA Inc., Concord, NC, USA) at a pressure of 0.3 MPa and a speed of 2 m/min. The resulting wet pick-up was 185 ± 5%. The fabric was transferred to 30 mL of an aqueous solution containing silver nitrate (14.7 mM) and ammonium hydroxide solution (60.5 mM) and agitated at room temperature for 15 min. The excess silver precursor solution was removed from the fabrics using the same padding method. The fabric was then transferred into 50 mL of an aqueous L-ascorbic acid solution, in which the fabric immediately turned brown in color. The obtained fabric was washed in DI water multiple times and air dried.

X-ray diffraction (XRD) spectra of pristine and Ag NP cotton fibers were collected using a PANalytical Empyrean X-ray Diffractometer (Malvern Panalytical, Malvern, UK) with CuK $\alpha$  radiation (1.54060 Å) and 45 kV and 40 mA for generator settings. Angular scanning was collected from 8.0 to 60° 2 $\theta$  with a step size of 0.03° and rate of 0.6°/min. X-ray photoelectron spectroscopy (XPS) measurements were collected using a VG Scientific ESCALAB MKII (Thermo Scientific, Waltham, MA, USA) spectrometer system using a Mono AlK $\alpha$  X-ray excitation source ( $h\nu = 1486.6$  eV) at 450 W power. The chamber pressure was below  $3 \times 10^{-9}$  mbar during analysis. Data acquisition was collected with 6 s dwell times per data point. The dwell time per data point was increased to 60 s per point for C1s and O1s, and 200 s per point for Ag3d to improve the signal-to-noise ratio at regions of interest. The signal of each data point was rescaled to dwell times of 60 s after data acquisition. The spectrum was calibrated by reference to the C 1s peak at 284.8 eV binding energy. All data was processed with Casa XPS software (Version 2.3.24, Casa Software, Ltd., Teignmouth, UK).

The uniform internal dispersion of Ag NPs within the cotton fiber was confirmed by a transmission electron microscope (TEM) (FEI Technai G2 F30) operating at 300 kV using a procedure developed at the Southern Regional Research Center located in New Orleans, LA, USA [29,30]. Fibers from the functionalized Ag NP-embedded cotton fabric were combed prior to immersion in a methacrylate matrix solution in Teflon tubing (3.2 mm inner diameter), and then polymerized under UV light for 30 min. The resulting block of coated fibers was removed from the tubing and subsequently immobilized in polyethylene capsules. The fibers were sectioned into 100–120 nm slices using a PowerTome Ultramicrotome (Boeckeler Instruments, Inc., Tucson, AZ, USA). The cross-sectioned slices were affixed to a copper grid coated with carbon film, and the polymer block was dissolved using methyl ethyl ketone.

The concentration of silver in the Ag NP cotton fabric was determined using inductively coupled plasma mass spectrometry (ICP-MS) at the University of Utah ICP-MS Metals Lab. UV/vis absorbance spectra were obtained of the Ag NP cotton for the wavelength range of 300 to 750 nm with a step size of 1.0 nm using a UV/vis/NIR spectrophotometer (ISR-2600, Shimadzu, Columbia, MA, USA). Origin 2018b Graphing and Analysis Software (OriginLab, Northampton, MA, USA) was used for analysis of spectral data.

## 2.3. Catalytic Degradation Studies and Turnover Determinations

Calibration curves were obtained for each dye within the range from 0.1 mg L<sup>-1</sup> to 50 mg L<sup>-1</sup> by UV/vis spectroscopy; for which 0.1 mg L<sup>-1</sup> is the limit of detection for each dye, and beyond 50 mg L<sup>-1</sup> the absorbance is overexposed and deviates from linearity. The UV/vis spectra were collected for a wavelength range of 300–750 nm and a step size

of 1.0 nm using a UV/vis/NIR spectrometer (ISR-2600, Shimadzu, Columbia, MA, USA). Acrylic cuvettes with a 1 cm optical path length filled with 3.0 mL solution were used.

For general catalytic degradation studies, 30.0 mg sodium borohydride ( $\text{NaBH}_4$ , 0.777 mmol) was dissolved in a 100 mL solution of 25 ppm dye (3.59  $\mu\text{mol}$  CR, 7.64  $\mu\text{mol}$  MO, 2.52  $\mu\text{mol}$  CSBB) and stirred using a magnetic stirrer bar at 180 rpm at room temperature. To this solution, either 200 mg or 400 mg Ag NPs–cotton catalyst (13,150 ppm Ag) was added, and the reaction time was started. The UV/vis spectrum at each timepoint was obtained by removing a 3.00 mL aliquot from the reaction solution and the spectra were collected immediately. The aliquot was readded to the reaction solution, maintaining an effective catalyst concentration throughout the duration of the reaction. The percentage dye concentration remaining was calculated by Equation (1), and Equation (2) gives the percentage degradation:

$$\text{percentage dye concentration} = \frac{[\text{dye}_t]}{[\text{dye}_0]} \times 100 \quad (1)$$

$$\text{percentage degradation} = \frac{[\text{dye}_0] - [\text{dye}_t]}{[\text{dye}_0]} \times 100 \quad (2)$$

where  $[\text{dye}_0]$  and  $[\text{dye}_t]$  are dye concentrations at time 0 and t, respectively, as determined using the aforementioned calibration curves.

The turnover number (TON) of the active catalyst was calculated by the methods employed previously [31,32] and is simply the moles of diazo bonds consumed per mole active site. The turnover frequency (TOF) is given by expressing the TON per unit time (min). To determine the number of active sites on a spherical Ag NP, the number of surface Ag atoms per NP, the number of NPs and finally the number of active sites per reaction must be calculated. The turnover frequency was determined for each dye using 200 mg and 400 mg Ag NP–cotton catalyst [33]. The lattice constant of a face-centered-cubic Ag nanocrystal is 0.409 nm and the volume of the unit cell is  $(0.409 \text{ nm})^3 = 0.068 \text{ nm}^3$ . Each unit cell of Ag contains four Ag atoms. Each Ag NP has a diameter of 9.7 nm and a radius (r) of 4.85 nm. The volume (V) of a Ag NP sphere is:

$$V = \frac{4}{3}\pi r^3 \approx 477.9 \text{ nm}^3 \quad (3)$$

Therefore, there are 28,036 Ag atoms per NP:

$$477.9 \text{ nm}^3 \frac{\text{unit cell}}{0.068 \text{ nm}^3} \times \frac{4 \text{ atoms}}{\text{unit cell}} \approx \frac{28,036 \text{ atoms}}{\text{NP}} \quad (4)$$

Given that any one face of the unit cell can face the surface of the NP, then there are two Ag atoms per surface area unit cell, which is  $(0.409 \text{ nm})^2 = 0.167 \text{ nm}^2$ . The surface area of the NP sphere is given by:

$$\text{Surface Area} = 4\pi r^2 \approx 296 \text{ nm}^2 \quad (5)$$

The number of Ag atoms (active sites) on the surface of each NP is given by the surface area of the sphere divided by the surface exposed unit cells times the number of Ag atoms per unit cell surface:

$$\frac{296 \text{ nm}^2}{0.167 \text{ nm}^2} \times 2 \text{ atoms} \approx \frac{3545 \text{ atoms}}{\text{NP}} \quad (6)$$

The number of active sites in the reaction, given the typical 200 mg fabric, was determined. The molecular mass of Ag (107.87 g/mol) with a catalyst load of 13.15 mg/g Ag in

cotton fabric, then there were ~2.631 mg Ag/reaction, which is ~24.4  $\mu\text{mol}$  Ag in reaction. From this the number of atoms of Ag can be determined using Avogadro's number:

$$\frac{24.4 \times 10^{-6} \text{ mol}}{\text{reaction}} \times \frac{6.02 \times 10^{23} \text{ atoms}}{\text{mol}} \approx \frac{1.47 \times 10^{19} \text{ atoms}}{\text{reaction}} \quad (7)$$

Since there were 28,036 Ag atoms per NP and there are  $1.47 \times 10^{19}$  Ag atoms per reaction, then there are  $5.24 \times 10^{14}$  Ag NP per reaction:

$$\frac{1.47 \times 10^{19} \text{ atoms}}{\text{reaction}} \times \frac{\text{NP}}{28,036 \text{ atoms}} \approx \frac{5.24 \times 10^{14} \text{ NP}}{\text{reaction}} \quad (8)$$

Given the number of Ag NP per reaction and the number of active sites per NP, it is then straightforward to determine the number of active sites and hence the number of moles of available Ag per reaction:

$$\frac{5.24 \times 10^{14} \text{ NP}}{\text{reaction}} \times \frac{3545 \text{ atoms}}{\text{NP}} \times \frac{\text{mol}}{6.02 \times 10^{23} \text{ atoms}} \approx \frac{3.08 \times 10^{-6} \text{ mol (active) Ag}}{\text{reaction}} \quad (9)$$

When the amount of fabric is doubled (400 mg), all other instances being equal, the available active sites per reaction also double since the number of NPs doubles and the average size of the NP and active sites per NP remain constant.

### 3. Results and Discussion

#### 3.1. Characterization of Ag NP–Cotton Catalyst

The UV/vis spectra of pristine white cotton and Ag NPs synthesized within cotton fibers (Figure 1a) as well as the digital microscope images at  $50\times$  magnification are shown in Figure 1a–c. When comparing the spectrum of unmodified pristine white cotton with that of the Ag NP cotton catalyst, the presence of a strong absorption band at 420 nm confirmed the formation of Ag NPs [34]. X-ray diffraction (XRD) and X-ray photoelectron spectroscopy (XPS) data confirm the addition of Ag NPs to the cotton fibers and the  $\text{Ag}^0$  valence state in Figures S1 and S2, respectively. Additionally, the change in color of the cotton fiber from white to yellow is consistent with the localized surface plasmon resonance of Ag NP formation within the cotton fiber [35]. Internal formation of the Ag NPs within the cotton fiber was confirmed by obtaining the TEM image of the Ag NP–cotton fiber cross-section, Figure 2c, and were observed to be uniformly distributed across the entire fiber diameter and exhibited a spherical morphology. The narrow size distribution for the Ag NPs,  $9.7 \pm 3.2$  nm, Figure 2a,b, can be attributed to the controlled particle growth within the cotton fiber along the cellulose chain [36]. As determined by ICP-MS following acid digestion of the resulting product, the Ag loading was 13.15 mg Ag per gram of cotton.

#### 3.2. Catalytic Activity Performance of Ag NP–Cotton

Owing to their remarkable surface area-to-volume ratio, spherical Ag NPs have been shown to have increased chemical reactivity as compared to their bulk metal counterparts because the smaller size results in a greater proportion of metal atoms residing at the surface [37,38]. Here, the catalytic capacity of the synthesized Ag NP–cotton catalyst is studied against the reduction of a mono-azo dye, MO, and two diazo dyes, CR and CSBB, using  $\text{NaBH}_4$  as an electron pair donor in aqueous medium. First, calibration curves for each dye from 50 ppm to 0.1 ppm were obtained by UV/vis spectroscopy to monitor the progress of dye degradation by the Ag NP–cotton catalyst, Figure 3. The UV/vis spectrum for MO is shown in Figure 3a. The strong absorption bands at 464 nm and 496 nm for MO and CR, respectively (Figure 3a,b), are assigned to the  $n\text{-}\pi^*$  transition of the  $\text{-N=N-}$  azo-nitrogen lone pair [39,40]. The strong absorption band at 618 nm for CSBB (Figure 3c) corresponds to the  $\pi\text{-}\pi^*$  transition of the  $\text{-N=N-}$  moiety [41,42]. The calibration curves derived from the UV/vis spectra are shown in Figure 3d–f. The decomposition of the dyes

by catalytic reduction results in the cleavage of the nitrogen–nitrogen bond and can be monitored by the decrease in the intensity of the respective absorption bands.

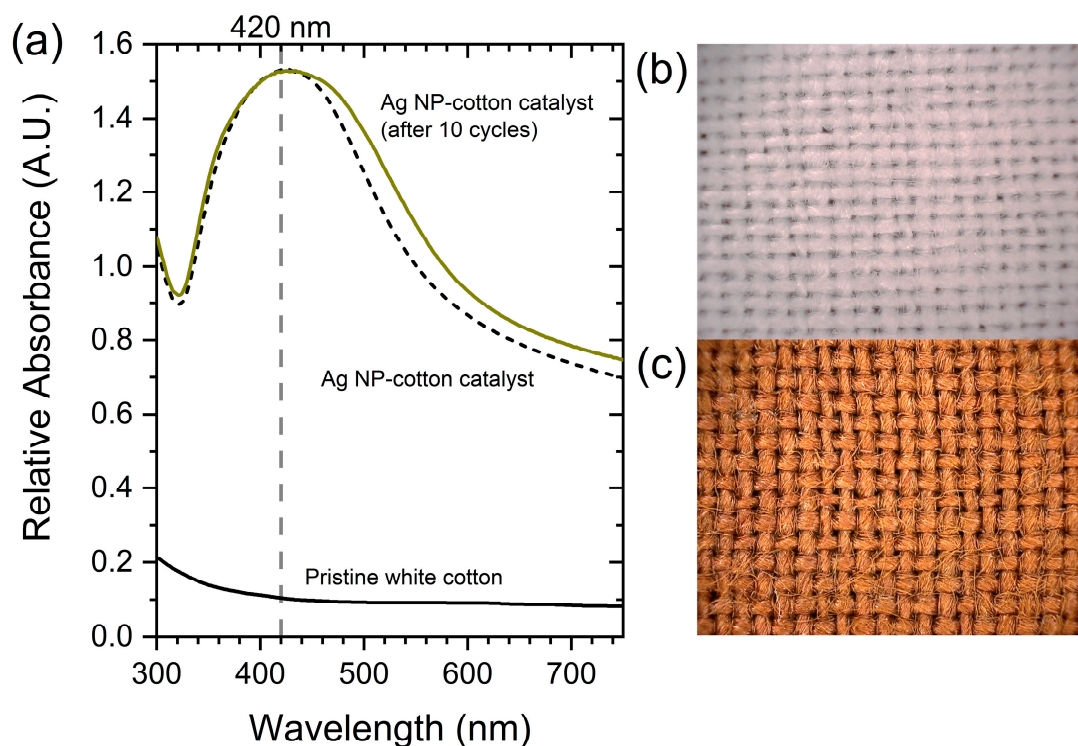


**Figure 1.** (a) UV/vis spectra of pristine white cotton (solid black line), synthesized Ag NP–cotton catalyst (solid yellow line) with maximum absorption at 420 nm, and Ag NP–cotton catalyst after 10 degradation cycles (dotted black line). Digital microscope images at 50 $\times$  magnification of (b) pristine white cotton fabric and (c) Ag NP–cotton catalyst fabric.

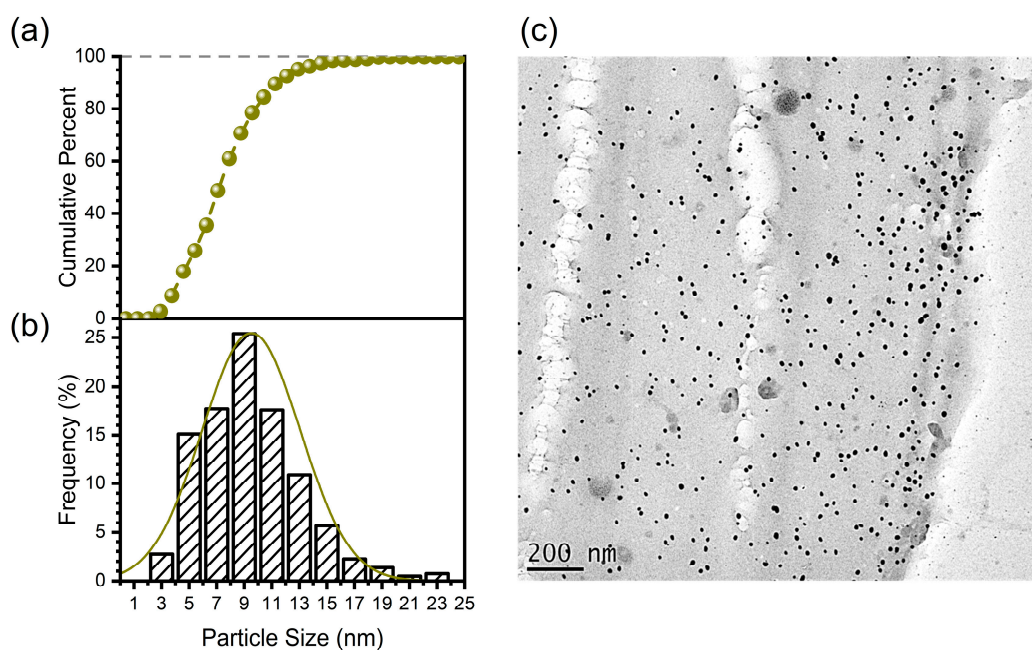


**Figure 2.** (a,b) Histogram and cumulative percentage of Ag NP size distribution ( $9.7 \pm 3.2$  nm) in the Ag NP–cotton catalyst as determined by (c) TEM image of the Ag NP–cotton catalyst fiber cross-section, confirming the internal formation and uniform distribution of Ag NPs within the entirety of the fiber.

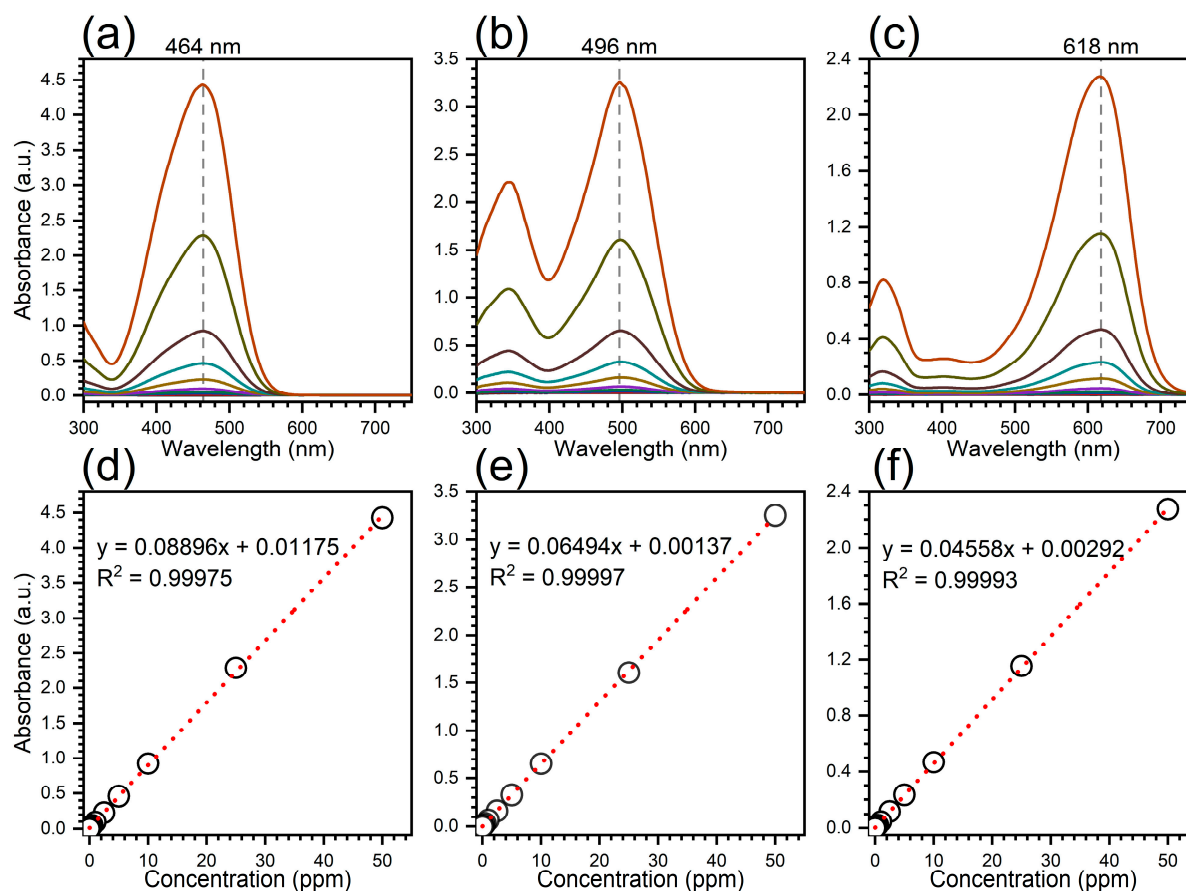


**Figure 3.** (a–c) UV/vis spectra of decreasing dye concentrations ( $\lambda_{max}$  denoted by the vertical dotted line) and (d–f) corresponding calibration curves with equations and linear regressions inset for methyl orange, Congo red, and Chicago Sky Blue 6B, respectively.

The effectiveness of the produced Ag NP–cotton fabric as a catalyst was studied via the catalytic reduction of azo  $-N=N-$  bonds in organic dyes. Initially, blank experiments were conducted to confirm that the dyes were not easily reduced by either  $\text{NaBH}_4$  or the Ag NP–cotton catalyst in the absence of the other. The reduction of the dyes by  $\text{NaBH}_4$  in the absence of the Ag NP–cotton catalyst proceeded slowly, with little change to the UV/vis spectra after several hours (Figures S3 and S4). Additionally, each dye was found to be stable in solution upon addition of Ag NP–cotton catalyst without  $\text{NaBH}_4$ , as determined by UV/vis spectroscopy. There have been several studies investigating the capability of Ag NPs as photocatalysts, capable of reducing azo  $-N=N-$  bonds of organic dyes in solution in the absence of an electron donor [43,44]. However, due to the Ag NPs being in the interior of the cotton fiber, light radiation is unable to penetrate through the cotton fiber and initiate the reaction.

Digital images were collected of the dye solutions before and after degradation studies, Figures S5–S7, showing by eye the effectiveness of the reaction to break down the organic dyes in solution. The UV/vis spectra as a function of time for MO is given in Figure 4a using 200 mg Ag NP–cotton catalyst. The absorption band at 464 nm decreased over 90 min with 99.3% dye degradation, Figure 4d. The reaction continued to slowly approach total degradation beyond this time. A proposed catalytic mechanism is presented in Scheme 1 [45,46]. Briefly, the electron-rich azo  $-N=N-$  double bond coordinates with a surface Ag atom, resulting in inductive electron withdrawal away from the dye nitrogen atom. Subsequently, the nitrogen atom undergoes nucleophilic attack by an electron donor hydride from  $\text{BH}_4^-$ , which is coulombically attracted to the positively charged surface of the Ag NPs, reducing the  $N=N$  double bond to a single bond. A second nucleophilic

attack by an electron donor hydride from  $\text{NaBH}_4$  results in the cleavage of the N–N single bond. Dissociation from the Ag surface produces the degradation products of sulfanilate and *N,N*-dimethyl-*p*-phenylenediamine, and regenerates the Ag NP–cotton catalyst. These degradation products do not interfere with accurate UV/vis measurements since they do not absorb between 300 nm and 750 nm.

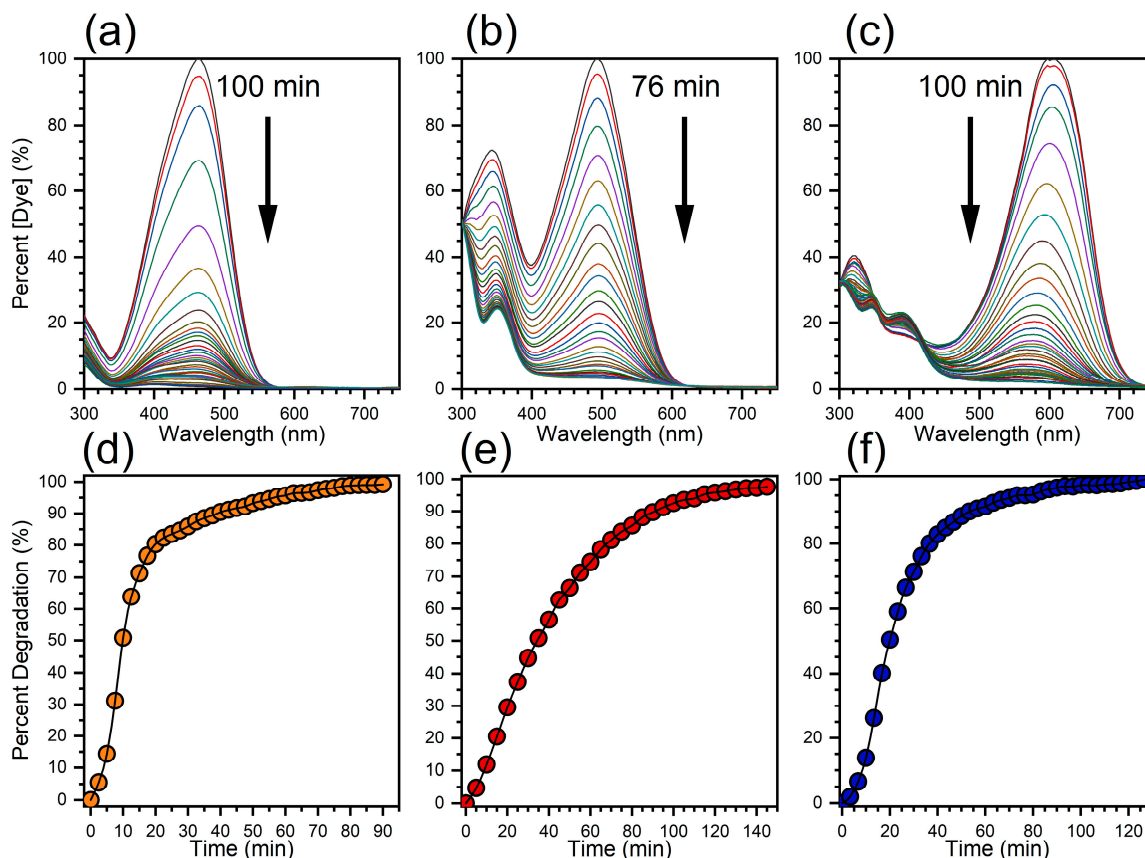
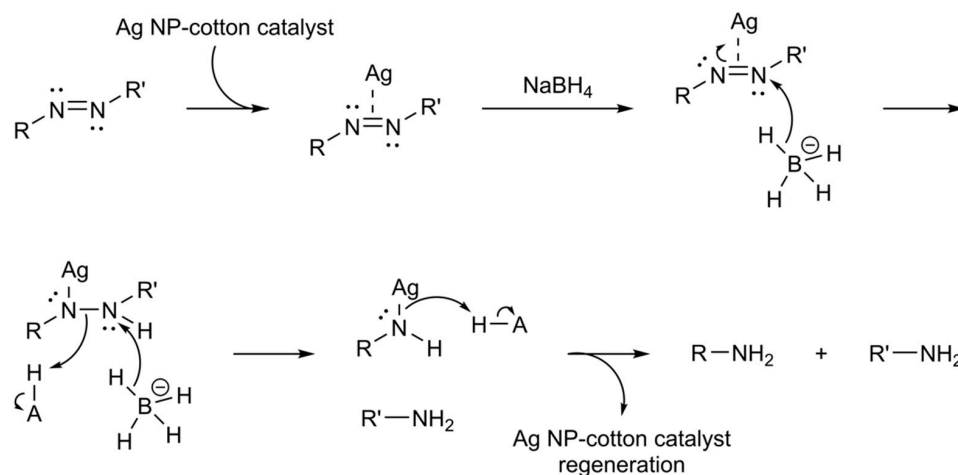


**Figure 4.** (a–c) UV/vis spectra for percentage dye concentration remaining, and (d–f) time plots of percent dye degradation for the catalytic reduction of MO, CR, and CSBB, respectively, by  $\text{NaBH}_4$  in the presence of 200 mg Ag NP–cotton.

#### Catalytic reaction mechanism



**Scheme 1.** Plausible mechanism for the Ag-catalytic reduction of azo-dyes by  $\text{NaBH}_4$ , where R and R' represent carbon-based functional groups, and H–A represents water as a proton source.



The catalytic reduction of the diazo dyes, CR and CSBB, were also monitored by UV/vis spectroscopy at 496 nm and 618 nm, respectively. Under the same conditions, 97.6% and 100% of the dyes were degraded after 145 min and 125 min, respectively (Figure 4b,e and Figure 4c,f, respectively). The longer reaction time for CR and CSBB can be attributed to the presence of two azo moieties in the chemical structure of the molecules. Although the molecular weights of CR and CSBB are greater than that of MO, the presence of two functional groups in close proximity can lead to steric hinderance for reactants in solution. However, the proximity of these functional groups on either side of the central biphenyl synergistically enhances the affinity to the Ag NP surface. As a result, the overall percentage degradation of these dyes was nearly equal to the single azo  $-N=N-$  of MO. The TOF was determined for each dye in the dye degradation time plots, and presented in Table 2. For the diazo dyes, the TOF was nearly half of that for MO, at  $0.019 \text{ min}^{-1}$  and  $0.021 \text{ min}^{-1}$  compared to  $0.041 \text{ min}^{-1}$ .

**Table 2.** Calculated turnover number (TON) and turnover frequency (TOF) for catalytic dye degradation studies using 200 and 400 mg Ag NP–cotton catalyst loading.

Dye	Ag NP–Cotton Catalyst Loading	Time (min) <sup>a</sup>	TON <sup>a</sup>	TOF ( $\text{min}^{-1}$ ) <sup>a</sup>
MO	200 mg	57.5	2.4	0.041
CR	200 mg	115	2.2	0.019
CSBB	200 mg	73.3	1.6	0.021
MO	400 mg	25.5	1.2	0.046
CR	400 mg	13.9	1.1	0.082
CSBB	400 mg	14.0	0.8	0.056

<sup>a</sup> Calculations based on  $\geq 95\%$  dye degradation (linear region).

The effect of Ag NP–cotton catalyst concentration was investigated by doubling the catalyst loading to 400 mg. The amount of time to complete the reaction significantly decreased for each dye. The degradation of MO reached 96.4% after only 30 min (Figure 5a,d), comparable with the percentage degradation after 90 min using half the catalyst loading. Interestingly, the enhanced reaction rate was most noticeable for the diazo dyes, CR and CSBB (Figure 5b,e and Figure 5c,f, respectively), suggesting their greater affinities assisted in the catalytic reduction by  $\text{NaBH}_4$ . However, notably time plots versus percentage degradation for CR and CSBB (Figure 5e,f) exhibit sigmoidal shapes. There is an initial lag in the increase of degradation product. This may be due to the presence of two azo  $-N=N-$  moieties where the molar absorptivity of the mono-reduced product is different to that of the diazo product, and therefore the linear region is not reached until only the mono-reduced azo degradation product is present in solution. Unlike 200 mg Ag NP catalyst loading, the TOFs for CR and CSBB,  $0.082 \text{ min}^{-1}$  and  $0.056 \text{ min}^{-1}$ , respectively, are greater than that of MO ( $0.046 \text{ min}^{-1}$ ).

### 3.3. Effect of pH on Catalytic Performance

The effect of solution pH on the degradation of MO, CR, and CSBB by  $\text{NaBH}_4$  using 200 mg Ag NP–cotton catalyst was investigated. Due to the use of  $\text{NaBH}_4$  as a reducing agent, the pH cannot be lowered as it would result in the evolution of hydrogen gas.  $\text{NaOH}$  was added to the dye solutions to adjust the pH to 9. Slightly decreased reaction times were observed for both MO and CSBB in more alkaline solutions, Figure 6, consistent with previous studies [46,47]. The surface of Ag NPs becomes negatively charged at pH values greater than 8, resulting in electrostatic repulsion between the NP surface and dye. Alternatively, CR showed enhanced reactivity with a decrease in reaction time from 145 to 76 min. Comparing the chemical structures for each of the dyes, MO is minimally affected by the change in pH due to the absence of alkaline sensitive functional groups [46]. Acidic phenylamines are present adjacent to the diazo bond for CR, allowing for electron donating character through resonance, increasing the reactivity for diazo bond degradation. However, CSBB does not have increased reactivity due to the two electron withdrawing sulfate groups on the naphthalene moieties.

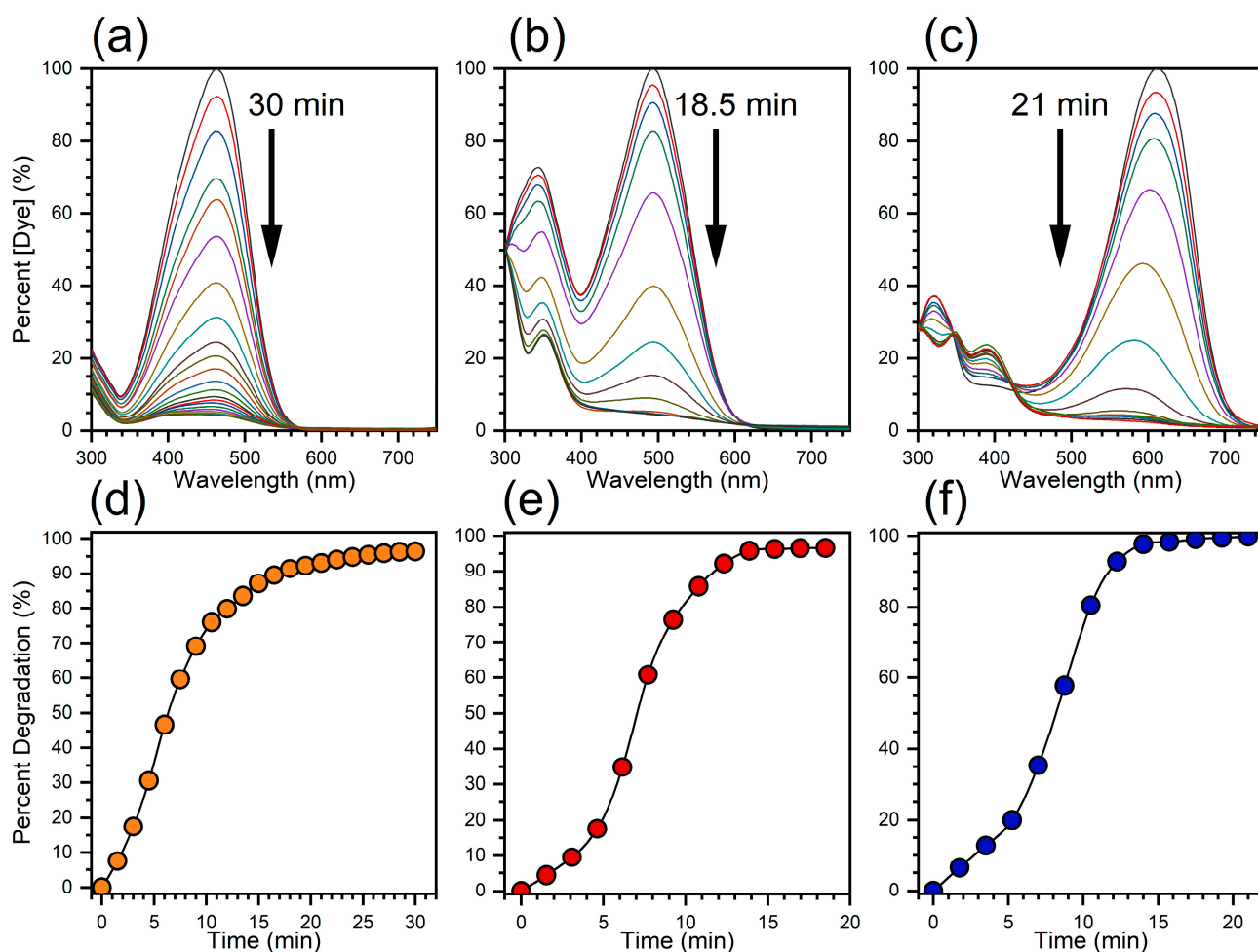


**Figure 5.** (a–c) UV/vis spectra of percentage dye concentration remaining, and (d–f) time plots of percentage dye degradation for the catalytic reduction of MO, CR, and CSBB, respectively, by  $\text{NaBH}_4$  in the presence of 400 mg Ag NP–cotton.

### 3.4. Recyclability of Ag NP–Cotton Catalyst

With the Ag NPs produced within the cotton fiber, the Ag NP–cotton catalyst can be easily removed from the reaction solution using tweezers and was then rinsed. Thus, to study the recyclability of the Ag NP catalyst, the same catalyst was used for the catalytic degradation for each dye over 10 cycles. The catalyst maintained very high efficiency (>95% degradation) after 10 cycles (Figure 7). While pristine white cotton fabric permanently changed to the corresponding dye color when immersed in the solution, the Ag NP–cotton catalyst fabric did not change color. Additionally, previous studies have shown that the Ag NPs are well secured within the cotton fiber and are resistant to NP leaching even under aggressive agitation, losing less than 20% of their overall Ag content after 50 laundering cycles. Due to the mild reaction conditions (room temperature and mild mixing by magnetic stirring) it is expected that the catalyst maintains its high silver loading for the lifetime of the fiber [36,48,49], as confirmed by the lack of change in the UV/vis spectrum of the Ag NP–cotton catalyst after 10 cycles (Figure 1).

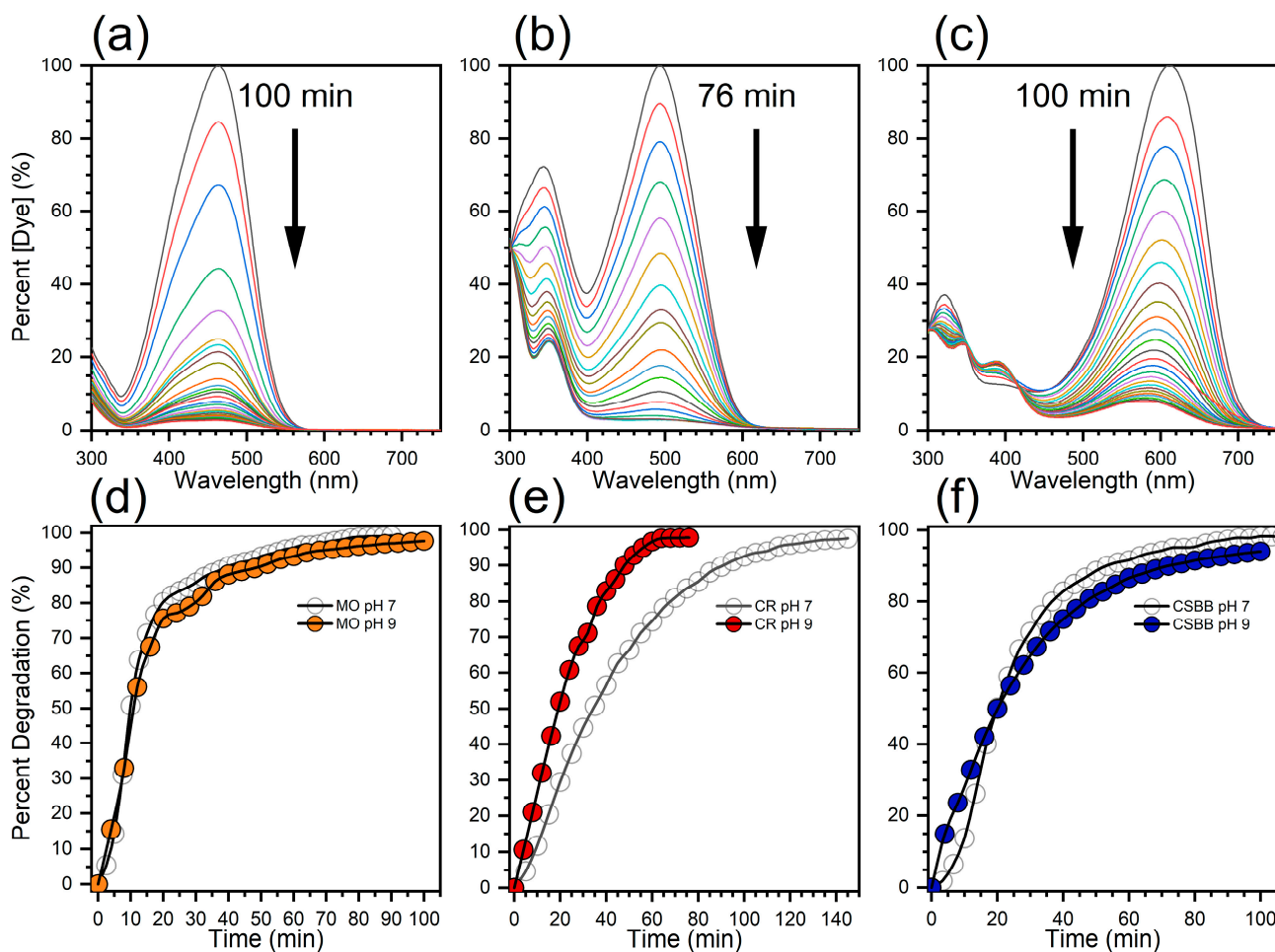


**Figure 6.** (a–c) UV/vis spectra of percentage dye concentration remaining, and (d–f) time plots of percentage dye degradation for the catalytic reduction of MO, CR, and CSBB, respectively, by  $\text{NaBH}_4$  in the presence of 200 mg Ag NP–cotton at pH 9.

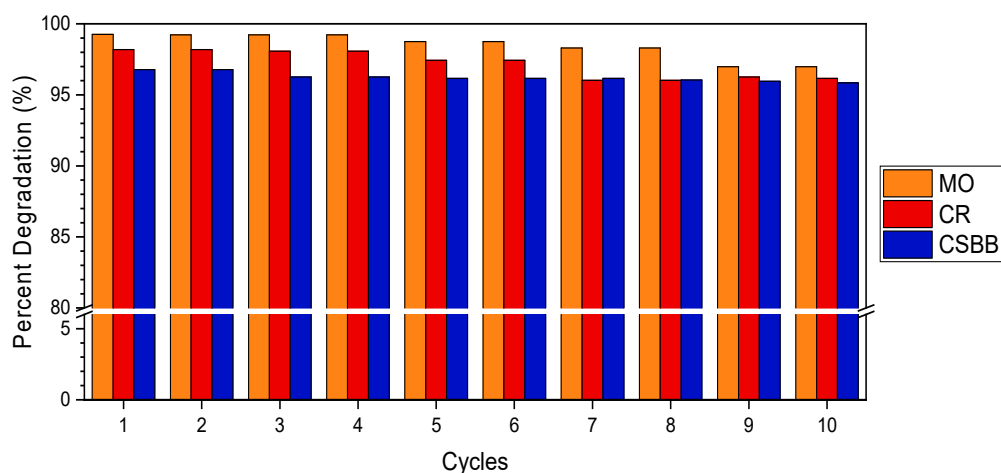


**Figure 7.** Catalytic activity of Ag NP–cotton catalyst against consecutive degradation reaction cycles.

#### 4. Conclusions

This study has shown that internally synthesized Ag NPs within cotton fiber can be used as an effective and efficient catalyst in the reduction of organic azo dyes by  $\text{NaBH}_4$ . The reaction was monitored by observing the decrease in the  $-\text{N}=\text{N}-$  absorption bands in the UV/vis spectra. The Ag NP–cotton catalyst was able to degrade highly concentrated

solutions of three different azo dyes, a mono-azo and two diazo containing dyes, within a reasonable amount of time. Comparing these results with previous studies, Table S1, this study demonstrated the capacity of the Ag NP–cotton catalyst to degrade a large volume of organic dye contaminant with relatively low loading. The concentration of the catalyst had a significant effect on the reaction rate, decreasing the overall reaction time and doubling the TOF. Additionally, the recyclability of the Ag NP–cotton catalyst was demonstrated, with little loss in the catalytic efficacy after 10 cycles. The percentage degradation for each dye after 10 cycles was maintained at greater than 95%. This study opens the possibility for a myriad of applications for this Ag NP-embedded cotton catalyst in dye remediation.

**Supplementary Materials:** The following supporting information can be downloaded at: <https://www.mdpi.com/article/10.3390/nano12101621/s1>, Figure S1: XRD spectra of pristine white cotton, mercerized white cotton, and Ag NP cotton catalyst; Figure S2: XPS spectra of pristine white cotton and Ag NP cotton catalyst; Figure S3: UV/vis spectra and overlay of percent degradation of dyes for NaBH<sub>4</sub> control at pH 7; Figure S4: UV/vis spectra and overlay of percent degradation of dyes for NaBH<sub>4</sub> control at pH 9; Figure S5: Digital image of degradation reactions before and after for MO; Figure S6: Digital image of degradation reactions before and after for CR; Figure S7: Digital image of degradation reactions before and after for CSBB; Table S1: Comparison of degradation reaction conditions for this study and others similarly performed in the literature. References [26,46,50,51] are cited in the Supplementary Materials.

**Author Contributions:** Conceptualization, M.B.H., J.H.J. and S.N.; methodology, M.B.H., J.H.J. and S.N.; software, M.B.H. and J.H.J.; validation, M.B.H., J.H.J. and S.N.; formal analysis, M.B.H. and J.H.J.; investigation, M.B.H., J.H.J. and S.N.; resources, M.B.H. and S.N.; data curation, M.B.H. and J.H.J.; writing—original draft preparation, M.B.H. and J.H.J.; writing—review and editing, M.B.H., J.H.J., S.N., M.W.E. and B.D.C.; visualization, M.B.H. and J.H.J.; supervision, S.N., M.W.E. and B.D.C.; project administration, S.N., M.W.E. and B.D.C.; funding acquisition, S.N., M.W.E. and B.D.C. All authors have read and agreed to the published version of the manuscript.

**Funding:** This research was funded through support by the United States Department of Agriculture—Agricultural Research Service.

**Institutional Review Board Statement:** Not applicable.

**Informed Consent Statement:** Not applicable.

**Conflicts of Interest:** The authors declare no conflict of interest.

## References

1. Ajiboye, T.O.; Oyewo, O.A.; Onwudiwe, D.C. Simultaneous removal of organics and heavy metals from industrial wastewater: A review. *Chemosphere* **2021**, *262*, 128379. [[CrossRef](#)] [[PubMed](#)]
2. Pirkarami, A.; Olya, M.E. Removal of dye from industrial wastewater with an emphasis on improving economic efficiency and degradation mechanism. *J. Saudi Chem. Soc.* **2017**, *21*, S179–S186. [[CrossRef](#)]
3. van Loosdrecht, M.C.; Brdjanovic, D. Water treatment. Anticipating the next century of wastewater treatment. *Science* **2014**, *344*, 1452–1453. [[CrossRef](#)] [[PubMed](#)]
4. Kuenemann, M.A.; Szymczyk, M.; Chen, Y.; Sultana, N.; Hinks, D.; Freeman, H.S.; Williams, A.J.; Fourches, D.; Vinueza, N.R. Weaver's historic accessible collection of synthetic dyes: A cheminformatics analysis. *Chem. Sci.* **2017**, *8*, 4334–4339. [[CrossRef](#)] [[PubMed](#)]
5. Liu, H.; Li, G.; Qu, J.; Liu, H. Degradation of azo dye Acid Orange 7 in water by Fe<sup>0</sup>/granular activated carbon system in the presence of ultrasound. *J. Hazard. Mater.* **2007**, *144*, 180–186. [[CrossRef](#)] [[PubMed](#)]
6. Rawat, D.; Mishra, V.; Sharma, R.S. Detoxification of azo dyes in the context of environmental processes. *Chemosphere* **2016**, *155*, 591–605. [[CrossRef](#)] [[PubMed](#)]
7. de Jong, L.; Pech, N.; de Aragao Umbuzeiro, G.; Moreau, X. Multi-scale biomarker evaluation of the toxicity of a commercial azo dye (Disperse Red 1) in an animal model, the freshwater cnidarian *Hydra attenuata*. *Water Res.* **2016**, *96*, 62–73. [[CrossRef](#)]
8. Hernandez-Zamora, M.; Martinez-Jeronimo, F. Congo red dye diversely affects organisms of different trophic levels: A comparative study with microalgae, cladocerans, and zebrafish embryos. *Environ. Sci. Pollut. Res. Int.* **2019**, *26*, 11743–11755. [[CrossRef](#)]
9. Abe, F.R.; Soares, A.; Oliveira, D.P.; Gravato, C. Toxicity of dyes to zebrafish at the biochemical level: Cellular energy allocation and neurotoxicity. *Environ. Pollut.* **2018**, *235*, 255–262. [[CrossRef](#)]

10. Mathieu-Denoncourt, J.; Martyniuk, C.J.; de Solla, S.R.; Balakrishnan, V.K.; Langlois, V.S. Sediment contaminated with the Azo Dye disperse yellow 7 alters cellular stress- and androgen-related transcription in *Silurana tropicalis* larvae. *Environ. Sci. Technol.* **2014**, *48*, 2952–2961. [[CrossRef](#)]
11. Tkaczyk, A.; Mitrowska, K.; Posyniak, A. Synthetic organic dyes as contaminants of the aquatic environment and their implications for ecosystems: A review. *Sci. Total Environ.* **2020**, *717*, 137222. [[CrossRef](#)] [[PubMed](#)]
12. Wintgens, V.; Dalmas, F.; Sebillé, B.; Amiel, C. Novel phosphorus-containing cyclodextrin polymers and their affinity for calcium cations and hydroxyapatite. *Carbohydr. Polym.* **2013**, *98*, 896–904. [[CrossRef](#)] [[PubMed](#)]
13. Hanis, K.K.A.; Muhammad Nasri, A.R.; Wan Farahiyah, W.K.; Mohd Rabani, M.Y. Bacterial Degradation of Azo Dye Congo Red by *Bacillus* sp. *J. Phys. Conf. Ser.* **2020**, *1529*, 022048. [[CrossRef](#)]
14. Berradi, M.; Hsissou, R.; Khudhair, M.; Assouag, M.; Cherkaoui, O.; El Bachiri, A.; El Harfi, A. Textile finishing dyes and their Impact on aquatic environs. *Heliyon* **2019**, *5*, e02711. [[CrossRef](#)] [[PubMed](#)]
15. Ribeiro, A.R.; Umbuzeiro, G.A. Effects of a textile azo dye on mortality, regeneration, and reproductive performance of the planarian, *Girardia tigrina*. *Environ. Sci. Eur.* **2014**, *26*, 22. [[CrossRef](#)] [[PubMed](#)]
16. Ferraz, E.R.; Umbuzeiro, G.A.; de-Almeida, G.; Caloto-Oliveira, A.; Chequer, F.M.; Zanoni, M.V.; Dorta, D.J.; Oliveira, D.P. Differential toxicity of Disperse Red 1 and Disperse Red 13 in the Ames test, HepG2 cytotoxicity assay, and *Daphnia* acute toxicity test. *Environ. Toxicol.* **2011**, *26*, 489–497. [[CrossRef](#)]
17. Chung, K.T. Azo dyes and human health: A review. *J. Environ. Sci. Health C Environ. Carcinog. Ecotoxicol. Rev.* **2016**, *34*, 233–261. [[CrossRef](#)]
18. Su, J.C.; Horton, J.J. Allergic contact dermatitis from azo dyes. *Australas. J. Dermatol.* **1998**, *39*, 48–49. [[CrossRef](#)]
19. Brown, T.; Slack, R.; Rushton, L.; British Occupational Cancer Burden Study, G. Occupational cancer in Britain. Urinary tract cancers: Bladder and kidney. *Br. J. Cancer* **2012**, *107* (Suppl. 1), S76–S84. [[CrossRef](#)]
20. Diacu, E. Colors: Properties and Determination of Synthetic Pigments. In *Encyclopedia of Food and Health*; Caballero, B., Finglas, P.M., Toldrá, F., Eds.; Academic Press: Cambridge, MA, USA, 2016; pp. 284–290. [[CrossRef](#)]
21. Didier de Vasconcelos, G.M.; Mulinari, J.; de Arruda Guelli Ulson de Souza, S.M.; Ulson de Souza, A.A.; de Oliveira, D.; de Andrade, C.J. Biodegradation of azo dye-containing wastewater by activated sludge: A critical review. *World J. Microbiol. Biotechnol.* **2021**, *37*, 101. [[CrossRef](#)]
22. Crini, G.; Lichtfouse, E. Advantages and disadvantages of techniques used for wastewater treatment. *Environ. Chem. Lett.* **2018**, *17*, 145–155. [[CrossRef](#)]
23. Varjani, S.; Rakholiya, P.; Ng, H.Y.; You, S.; Teixeira, J.A. Microbial degradation of dyes: An overview. *Bioresour. Technol.* **2020**, *314*, 123728. [[CrossRef](#)] [[PubMed](#)]
24. Vidhu, V.K.; Philip, D. Catalytic degradation of organic dyes using biosynthesized silver nanoparticles. *Micron* **2014**, *56*, 54–62. [[CrossRef](#)] [[PubMed](#)]
25. Vanaamudan, A.; Sadhu, M.; Pamidimukkala, P. Chitosan-Guar gum blend silver nanoparticle bionanocomposite with potential for catalytic degradation of dyes and catalytic reduction of nitrophenol. *J. Mol. Liq.* **2018**, *271*, 202–208. [[CrossRef](#)]
26. Kolya, H.; Maiti, P.; Pandey, A.; Tripathy, T. Green synthesis of silver nanoparticles with antimicrobial and azo dye (Congo red) degradation properties using *Amaranthus gangeticus* Linn leaf extract. *J. Anal. Sci. Technol.* **2015**, *6*, 33. [[CrossRef](#)]
27. Aryan; Ruby; Mehata, M.S. Green synthesis of silver nanoparticles using *Kalanchoe pinnata* leaves (life plant) and their antibacterial and photocatalytic activities. *Chem. Phys. Lett.* **2021**, *778*, 138760. [[CrossRef](#)]
28. Nam, S.; Condon, B.D. Internally dispersed synthesis of uniform silver nanoparticles via in situ reduction of  $[\text{Ag}(\text{NH}_3)_2]^+$  along natural microfibrillar substructures of cotton fiber. *Cellulose* **2014**, *21*, 2963–2972. [[CrossRef](#)]
29. Boylston, E.K.; Hinojosa, O.; Hebert, J.J. A quick embedding method for light and electron microscopy of textile fibers. *Biotech. Histochem.* **1991**, *66*, 122–124. [[CrossRef](#)]
30. Thibodeaux, D.P.; Evans, J.P. Cotton Fiber Maturity by Image Analysis. *Text. Res. J.* **2016**, *56*, 130–139. [[CrossRef](#)]
31. Sreedhala, S.; Sudheeshkumar, V.; Vinod, C.P. Structure sensitive chemical reactivity by palladium concave nanocubes and nanoflowers synthesised by a seed mediated procedure in aqueous medium. *Nanoscale* **2014**, *6*, 7496–7502. [[CrossRef](#)]
32. Hong, K.; Sajjadi, M.; Suh, J.M.; Zhang, K.; Nasrollahzadeh, M.; Jang, H.W.; Varma, R.S.; Shokouhimehr, M. Palladium Nanoparticles on Assorted Nanostructured Supports: Applications for Suzuki, Heck, and Sonogashira Cross-Coupling Reactions. *ACS Appl. Nano Mater.* **2020**, *3*, 2070–2103. [[CrossRef](#)]
33. Easson, M.; Jordan, J.H.; Bland, J.M.; Hinchliffe, D.J.; Condon, B.D. Application of Brown Cotton-Supported Palladium Nanoparticles in Suzuki-Miyaura Cross-Coupling Reactions. *ACS Appl. Nano Mater.* **2020**, *3*, 6304–6309. [[CrossRef](#)]
34. Slistan-Grijalva, A.; Herrera-Urbina, R.; Rivas-Silva, J.F.; Avalos-Borja, M.; Castellón-Barraza, F.F.; Posada-Amarillas, A. Assessment of growth of silver nanoparticles synthesized from an ethylene glycol–silver nitrate–polyvinylpyrrolidone solution. *Phys. E Low-Dimens. Syst. Nanostruct.* **2005**, *25*, 438–448. [[CrossRef](#)]
35. Chen, Y.; Ge, F.; Guang, S.; Cai, Z. Self-assembly of Ag nanoparticles on the woven cotton fabrics as mechanical flexible substrates for surface enhanced Raman scattering. *J. Alloys Compd.* **2017**, *726*, 484–489. [[CrossRef](#)]
36. Hillyer, M.B.; Nam, S.; Condon, B.D. Quantification and spatial resolution of silver nanoparticles in cotton textiles by surface-enhanced Raman spectroscopy (SERS). *J. Nanopart. Res.* **2020**, *22*, 42. [[CrossRef](#)]
37. Hamouda, R.A.; Hussein, M.H.; Abo-Elmagd, R.A.; Bawazir, S.S. Synthesis and biological characterization of silver nanoparticles derived from the cyanobacterium *Oscillatoria limnetica*. *Sci. Rep.* **2019**, *9*, 13071. [[CrossRef](#)]

38. Lowry, G.V.; Gregory, K.B.; Apte, S.C.; Lead, J.R. Transformations of nanomaterials in the environment. *Environ. Sci. Technol.* **2012**, *46*, 6893–6899. [[CrossRef](#)]
39. Lin, X.; Huang, T.; Huang, F.; Wang, W.; Shi, J. Photocatalytic activity of a Bi-based oxychloride  $\text{Bi}_4\text{NbO}_8\text{Cl}$ . *J. Mater. Chem.* **2007**, *17*, 138–146. [[CrossRef](#)]
40. Bhat, S.S.M.; Sundaram, N.G. Efficient visible light photocatalysis of  $\text{Bi}_4\text{TaO}_8\text{Cl}$  nanoparticles synthesized by solution combustion technique. *RSC Adv.* **2013**, *3*, 14371–14378. [[CrossRef](#)]
41. Green, F.J. *The Sigma-Aldrich Handbook of Stains, Dyes, and Indicators*; Aldrich Chemical Co.: Milwaukee, WI, USA, 1990; p. 1000.
42. Advincula, R.C.; Fells, E.; Park, M.-k. Molecularly Ordered Low Molecular Weight Azobenzene Dyes and Polycation Alternate Multilayer Films: Aggregation, Layer Order, and Photoalignment. *Chem. Mater.* **2001**, *13*, 2870–2878. [[CrossRef](#)]
43. Marimuthu, S.; Antonisamy, A.J.; Malayandi, S.; Rajendran, K.; Tsai, P.C.; Pugazhendhi, A.; Ponnusamy, V.K. Silver nanoparticles in dye effluent treatment: A review on synthesis, treatment methods, mechanisms, photocatalytic degradation, toxic effects and mitigation of toxicity. *J. Photochem. Photobiol. B* **2020**, *205*, 111823. [[CrossRef](#)] [[PubMed](#)]
44. Murugadoss, G.; Kumar, D.D.; Kumar, M.R.; Venkatesh, N.; Sakthivel, P. Silver decorated  $\text{CeO}_2$  nanoparticles for rapid photocatalytic degradation of textile rose bengal dye. *Sci. Rep.* **2021**, *11*, 1080. [[CrossRef](#)] [[PubMed](#)]
45. Wadhvani, S.A.; Shedbalkar, U.U.; Nadhe, S.; Singh, R.; Chopade, B.A. Decolorization of textile dyes by combination of gold nanocatalysts obtained from *Acinetobacter* sp. SW30 and  $\text{NaBH}_4$ . *Environ. Technol. Innov.* **2018**, *9*, 186–197. [[CrossRef](#)]
46. Nagar, N.; Devra, V. A kinetic study on the degradation and biodegradability of silver nanoparticles catalyzed Methyl Orange and textile effluents. *Heliyon* **2019**, *5*, e01356. [[CrossRef](#)]
47. Bo, Z.J.; Zhang, L.J.; Yan, L.; Tian, H.S.; Wei, H. Oxidation of Methyl Orange Solution with Potassium Peroxydisulfate. *Iran. J. Chem. Chem. Eng.* **2012**, *31*, 21–24. [[CrossRef](#)]
48. Nam, S.; Hillyer, M.B.; Condon, B.D.; Lum, J.S.; Richards, M.N.; Zhang, Q. Silver Nanoparticle-Infused Cotton Fiber: Durability and Aqueous Release of Silver in Laundry Water. *J. Agric. Food Chem.* **2020**, *68*, 13231–13240. [[CrossRef](#)]
49. Nam, S.; Ernst, N.; Chavez, S.E.; Hillyer, M.B.; Condon, B.D.; Gibb, B.C.; Sun, L.; Guo, H.; He, L. Practical SERS method for assessment of the washing durability of textiles containing silver nanoparticles. *Anal. Methods* **2020**, *12*, 1186–1196. [[CrossRef](#)]
50. Bogireddy, N.K.R.; Kumar, H.A.K.; Mandal, B.K. Biofabricated silver nanoparticles as green catalyst in the degradation of different textile dyes. *J. Environ. Chem. Eng.* **2016**, *4*, 56–64. [[CrossRef](#)]
51. Albeladi, S.S.R.; Malik, M.A.; Al-Thabaiti, S.A. Facile biofabrication of silver nanoparticles using *Salvia officinalis* leaf extract and its catalytic activity towards Congo red dye degradation. *J. Mater. Res. Technol.* **2020**, *9*, 10031–10044. [[CrossRef](#)]